Influence of the anion on the spectroscopy and scintillation mechanism in pure and Ce^{3+}-doped K_2LaX_5 and LaX_3 (X=Cl, Br, I)

E. V. D. van Loef,[1] P. Dorenbos,[1] C. W. E. van Eijk,[1] K. W. Krämer,[2] and H. U. Güdel[2]
[1]*Interfaculty Reactor Institute, Delft University of Technology, Mekelweg 15, 2629 JB Delft, The Netherlands*
[2]*Department of Chemistry and Biochemistry, University of Bern, Freiestrasse 3, 3000 Bern 9, Switzerland*
(Received 14 March 2003; published 11 July 2003)

The optical properties and scintillation mechanism in pure and Ce^{3+}-doped K_2LaX_5 and LaX_3 have been determined under x-ray, γ-ray, vacuum ultraviolet light, and synchrotron radiation excitation. Special attention is paid to the influence of anions $X=Cl^-$, Br^-, and I^-, and a comparison is made with properties of pure and Eu^{2+}-doped KX compounds. The energies of the $5d$ excited states of Ce^{3+} have been determined, and the total crystal field splitting and the centroid shift are discussed. An excitation across the band gap creates a combination of self-trapped exciton (STE) and Ce^{3+} emission. These emissions are often anticorrelated when temperature or Ce^{3+} concentration is changed. Their ratio is related to the STE mobility and STE creation rate. Clear trends in the optical properties and scintillation mechanism are observed along the halide series.

DOI: 10.1103/PhysRevB.68.045108 PACS number(s): 78.55.Hx

I. INTRODUCTION

Industrial and technical applications have motivated the research and development of new inorganic scintillators for years. Attention has been given to Ce^{3+}-doped materials, the characterization of their optical and scintillation properties, and the elucidation of the scintillation mechanism.[1–4]

Recently, it was shown that especially the lanthanum halides $LaCl_3$ and $LaBr_3$ doped with Ce^{3+} have excellent scintillation properties.[5,6] Both have a high light yield, good energy resolution, and a fast scintillation decay under γ-ray excitation. A scintillation mechanism involving the role of self-trapped excitons in the energy transfer from the host to Ce^{3+} was proposed for $LaCl_3:Ce^{3+}$, recently.[7]

In an attempt to further investigate the influence of the chemical environment on the optical properties and scintillation mechanism of metal-halide scintillators, we decided to work on pure and Ce^{3+}-doped K_2LaX_5 (X=Cl, Br, I). These systems are isostructural, whereas the environment of the M^{3+} cation is altered by chemical variation of the halide anions from Cl to Br to I.

It is well known that the physical and chemical properties of the halogens and their anions change considerably along the series from F to Cl to Br to I. The anion has a profound influence on both the energy of the $5d$ levels of Ce^{3+},[8–10] and the luminescence properties of the pure compound. For instance, the emission energies and lifetimes of self-trapped excitons (STEs) in alkali halides strongly depend on the anion.[11] Also the dynamic properties of the STE change because, e.g., the energy barrier for STE migration through the lattice decreases from Cl to Br to I.

This work reports on the influence of the anion on the optical properties and scintillation mechanism of pure and Ce^{3+}-doped K_2LaX_5 with X=Cl, Br, and I. Both static and dynamic aspects are discussed. The spectroscopic properties of $K_2LaX_5:Ce^{3+}$ are compared to those of Ce^{3+} In $LaCl_3$, $LaBr_3$, and to lesser extent LaI_3, as well as of Eu^{2+} in the potassium halides KX. The emission wavelength and lifetime of the STE, the energy of the $4f5d$ states of Ce^{3+}, as well as energy transfer from the STE to Ce^{3+} are described and discussed.

II. EXPERIMENT

A. Synthesis and structure

Single crystals of pure and Ce^{3+}-doped K_2LaX_5 (X=Cl, Br, I) were grown by the vertical Bridgman technique using a static ampoule and a moving furnace. We used as starting materials KX (Merck, suprapur), LaX_3, and CeX_3. $LaCl_3$ and $LaBr_3$ and $CeCl_3$ and $CeBr_3$ were prepared from La_2O_3, using the ammonium halide method.[12,13] LaI_3 and CeI_3 were synthesized from the elements.[14] To remove traces of water and oxygen they were purified by sublimation in tantalum or silica ampoules. For the crystal growth, stoichiometric amounts of the starting materials were sealed in silica ampoules under vacuum. All material handling was done under strictly dry conditions, e.g., in glove boxes with less than 0.1 ppm H_2O.

The ternary halides K_2LaX_5 crystallize in the K_2PrX_5-type structure, space group Pnma (no. 62).[15] The structure can also be described as a hexagonal densest arrangement of chains of edge-connected polyhedra $[LaX_7]$. The polyhedra may be viewed as distorted monocapped trigonal prisms with the La^{3+} ion in the center, see Fig. 1. The point symmetry at the La site is C_s. The seven Cl^-, Br^-, or I^- ions are at an average distance of 284 pm, 299 pm, and 323 pm from the central La^{3+} ion, respectively. The

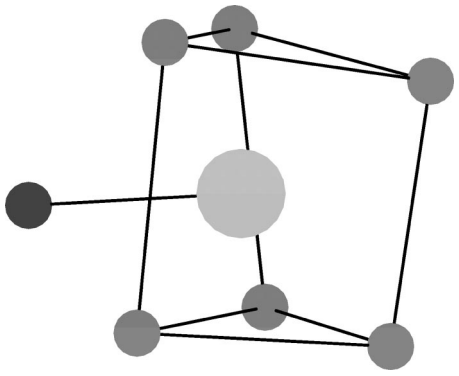

FIG. 1. The distorted monocapped trigonal prism polyhedron around La^{3+} in K_2LaCl_5.

calculated density of K_2LaCl_5, K_2LaBr_5, and K_2LaI_5 is 2.9 g/cm^3, 3.9 g/cm^3, and 4.4 g/cm^3, respectively.

B. X-ray excited luminescence spectra

An x-ray tube with Cu anode operating at 40 kV and 25 mA was used to generate x-ray excited luminescence spectra. The spectra were recorded with an ARC VM504 monochromator (blazed at 300 nm, 1200 grooves/mm) and a Hamamatsu R323 photomultiplier tube (PMT). The spectra in this study were corrected for the wavelength dependence of the photodetector quantum efficiency as well as monochromator transmission. The spectral resolution is typically 1 nm. Temperature dependent x-ray excited luminescence measurements were performed between 80 and 400 K, using a Cryospec model 20A Joule-Thomson Miniature Refrigerator operated with 99.999% nitrogen gas at 120 bar. The temperature was stabilized to within 0.1 K. The actual sample temperature is determined by the thermal coupling of the sample to the cooling device. We estimate an accuracy of about 5 K.

C. Excitation and emission spectroscopy

Excitation between 150 and 500 nm was done by means of an ARC DS-775 deuterium continuous discharge lamp and an ARC VM502 monochromator (blazed at 250 nm, 1200 grooves/mm). The emission spectra were recorded with a Macam 910 UV emission monochromator (blazed at 350 nm, 1200 grooves/mm) and a Philips XP2020Q PMT. The sample holder as well as the excitation monochromator are operated under vacuum. The spectra were corrected for the wavelength dependence of the photodetector quantum efficiency as well as monochromator transmission, using sodium salicylate as a reference.

High-resolution excitation and emission spectra at 10 K were recorded with synchrotron radiation at the SUPERLUMI station of the Synchrotron Strahlungslabor (HASYLAB) at the Deutsches Elektronen Synchrotron (DESY) in Hamburg (Germany). Details of this facility have been described elsewhere.[16] The spectral region of excitation was 50–335 nm with a fixed resolution of 0.3 nm. Luminescence was detected using a cooled Hamamatsu R2059 PMT. The resolution was 1 nm. The synchrotron operated in the multibunch regime (5 bunches) with 192 ns distance between successive bunches. Photons were counted within a time window of 27 ns at the start of the synchrotron luminescence pulse. Another time window of 106 ns duration was used at the end of the pulse to discriminate between fast and slow luminescence components. Also the integral count rate was recorded. Excitation spectra were corrected using sodium salicylate as a reference.

D. Scintillation decay and light yield measurements

Scintillation decay time spectra at time scales up to 10 μs were recorded by the multihit method described by Moses.[17] The crystals under study were mounted on a Philips XP2020Q ''start'' PMT. Single photons were detected by another Philips XP2020Q ''stop'' PMT. Both signals were transformed into fast logic pulses using an Ortec 934 constant fraction discriminator (CFD). The time differences between the ''start'' and the ''stop'' pulses are digitized using a LeCroy 4208 time-to-digital converter (TDC) and stored in a histogram.

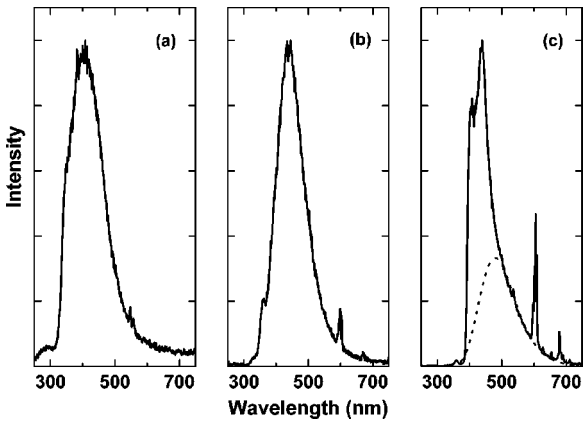

FIG. 2. X-ray excited luminescence spectra of (a) K_2LaCl_5, (b) K_2LaBr_5, and (c) K_2LaI_5 at 80 K. The dotted trace in the spectrum of K_2LaI_5 represents the contribution of STEs to the emission.

The absolute scintillation light yield at room temperature of K_2LaBr_5:0.7% Ce^{3+} and K_2LaI_5:0.7% Ce^{3+} was determined from the 662 keV total absorption peak in the pulse height spectrum of a ^{137}Cs source detected with the scintillation crystal mounted on a Hamamatsu R1791 photomultiplier tube. Standard spectroscopic techniques with a shaping time of 10 μs and employing the single photoelectron spectrum as reference were used. Further details can be found elsewhere.[18,19]

III. RESULTS

A. X-ray excited luminescence

Figure 2 shows the x-ray excited luminescence spectra of K_2LaX_5 (X=Cl, Br, I) at 80 K. The spectra are dominated by a broad emission band located between 300 and 550 nm. The emission band can readily be assigned to STE luminescence. For the iodides the emission spectrum of the STE is shown as the dotted trace. The sharp line emissions at 600 and 679 nm in the iodide spectrum and to a lesser extend in the bromide spectrum are probably due to not further identified rare earth impurities. The sharp decline of intensity in the K_2LaI_5 spectrum at wavelengths shorter than 400 nm is attributed to absorption of STE emission by the 380 nm *fd* transition of Ce^{3+} present as impurity in the nominally undoped compound. Ce^{3+} is also the origin for the emission bands observed near 400 and 440 nm. Unintended Ce^{3+} impurities are also the reason for some structure on the high-energy side of the STE emission in K_2LaCl_5 and K_2LaBr_5.

X-ray excited luminescence spectra of K_2LaCl_5:0.1% Ce^{3+},[20] K_2LaBr_5:0.7% Ce^{3+}, and K_2LaI_5:0.7% Ce^{3+} at 80 K are shown in Fig. 3 (solid traces). Also depicted are the 300 K spectra of the bromide and the iodide compounds (dotted traces). For all three lattices characteristic $Ce^{3+}5d \rightarrow 4f$ emission is observed. The maxima are located at 344 and 372 nm for the chloride, at 359 and 391 nm for the

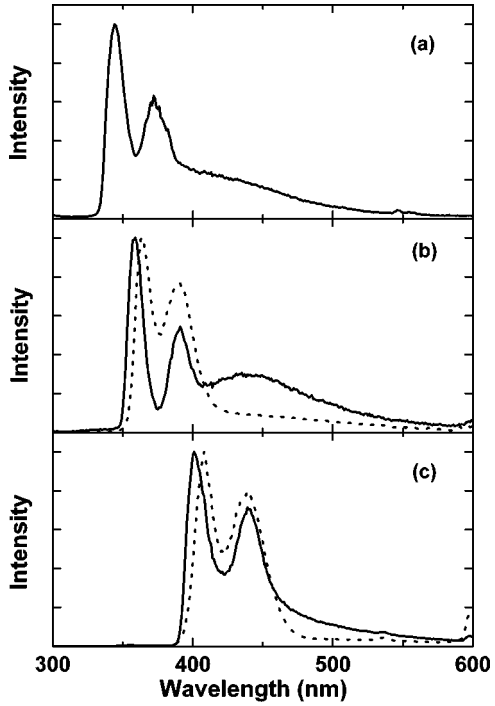

FIG. 3. X-ray excited luminescence spectra of (a) K_2LaCl_5:0.1% Ce^{3+}, (b) K_2LaBr_5:0.7% Ce^{3+}, and (c) K_2LaI_5:0.7% Ce^{3+}. The spectra were measured at 80 K (solid trace) and at 300 K (dotted trace).

bromide, and at 401 and 439 nm for the iodide for the $5d \rightarrow {}^2F_{5/2}$ and ${}^2F_{7/2}$ transitions, respectively. In addition, a weak emission is present as a broadband or tail on the long wavelength side of the Ce^{3+} doublet. It is attributed to residual STE emission. If the temperature is raised to 300 K, the intensity of this band decreases rapidly and only Ce^{3+} emission is observed.

The total luminescence intensity under x-ray excitation of K_2LaBr_5:0.7% Ce^{3+} and K_2LaI_5:0.7% Ce^{3+} is depicted in Figs. 4 and 5, respectively. From 100 to 175 K, the total luminescence intensity of the bromide and iodide decreases by about 14% and 22%, respectively. As the temperature rises the Ce^{3+} luminescence intensity is enhanced at the expense of STE luminescence intensity (compare with Fig. 3). Also the total luminescence intensity increases.

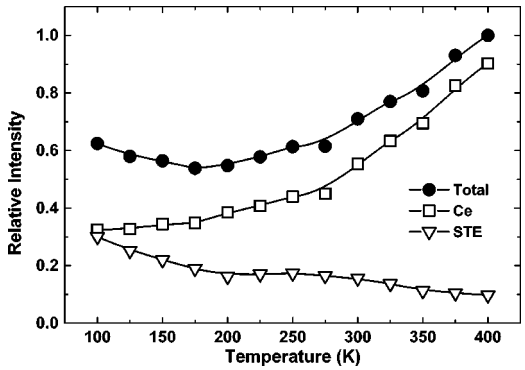

FIG. 4. Temperature dependence of Ce^{3+}, STE, and total luminescence intensity of x-ray excited K_2LaBr_5:0.7% Ce^{3+}.

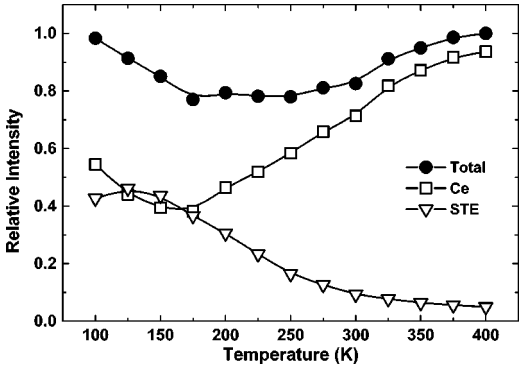

FIG. 5. Temperature dependence of Ce^{3+}, STE, and total luminescence intensity of x-ray excited K_2LaI_5:0.7% Ce^{3+}.

This anticorrelation between Ce^{3+} and STE luminescence has been observed more clearly in $LaCl_3$:0.57% Ce^{3+} by Guillot-Noël *et al.*[18] and in K_2LaCl_5:0.23% Ce^{3+} by van't Spijker *et al.*[20] It appears to be a general behavior in the K_2LaX_5 and LaX_3 systems. Furthermore, at 100 K the ratio of Ce^{3+} to STE emission increases along the series from Cl to I. At 100 K the contributions of Ce^{3+} and STE luminescence to the total intensity of K_2LaCl_5:0.23% Ce^{3+} are 15% and 85%, respectively.[18] However, for K_2LaBr_5:0.7% Ce^{3+} and K_2LaI_5:0.7% Ce^{3+} the contributions of Ce^{3+} and STE luminescence are almost equal. At 135 K this is also true for $LaCl_3$:0.57% Ce^{3+},[19] whereas for $LaBr_3$:Ce^{3+} the contribution of STE luminescence to the total luminescence intensity is negligible.[21]

The absolute scintillation light outputs determined from γ ray pulse height spectra were found to be 21 000, 26 000, and 52 000 photons per MeV of absorbed γ ray energy for K_2LaCl_5:0.7% Ce^{3+}, K_2LaBr_5:0.7% Ce^{3+}, and K_2LaI_5:0.7% Ce^{3+}, respectively. Measurements were performed at room temperature with a ^{137}Cs source using 10 μs shaping time. These numbers demonstrate that the energy transport from the host crystal to Ce^{3+} is very efficient in this class of materials.

B. Excitation and emission spectroscopy

Figure 6 compares the excitation spectra of STE emission in pure K_2LaCl_5 and K_2LaBr_5 at 10 K. We define three dif-

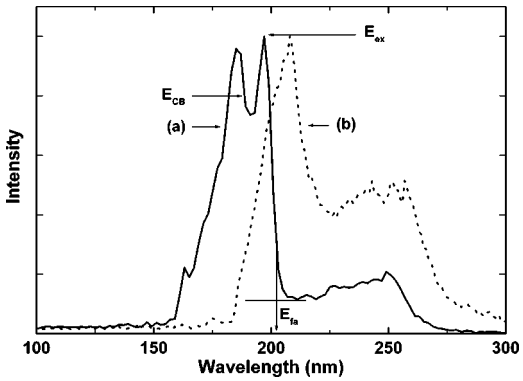

FIG. 6. Excitation spectra of (a) pure K_2LaCl_5 and (b) pure K_2LaBr_5 at 10 K monitoring STE luminescence at 415 and 400 nm, respectively.

TABLE I. Properties of undoped LaX_3, KX, and K_2LaX_5 (X = Cl, Br, I). Energies are in eV and wavelength λ_{STE} is in nm. For λ_{STE} the emission wavelength of the spin-forbidden π-polarized transition is compiled.

Compound	E_{fa}	E_{ex}	E_{CB}	λ_{STE}	Ref.
$LaCl_3$	6.2	6.5	≈7	405	22
$LaBr_3$	5.2	5.4	≈5.6	430	this work
LaI_3	3.2				this work
KCl	7.5	7.8	8.7	537(π)	24
KBr	6.4	6.7	7.4	544(π)	24
KI	5.8	5.9	6.3	407(π)	24
K_2LaCl_5	6.1	6.3	6.6	400	this work
K_2LaBr_5	4.9			440	this work
K_2LaI_5	3.9			≈480	this work

ferent energy values. The fundamental absorption E_{fa} is the energy of the first sharp onset in the excitation or absorption spectrum of the pure compound. For K_2LaCl_5 this is 202 nm (6.1 eV). The first maximum in the excitation spectrum of STE emission is attributed to the creation of free excitons that can be regarded as bound electron hole pairs. This exciton energy E_{ex} is located at 197 nm (6.3 eV).

For K_2LaCl_5 the edge of the conduction band E_{CB} is found at higher energy and corresponds to the creation of free electrons in the conduction band and free holes in the valence band. The second onset at 188 nm (6.6 eV) in the spectrum of K_2LaCl_5 is tentatively attributed to these across the band gap excitations. The data on band gap and exciton energies are compiled in Table I. Figure 6 also shows some excitation at energies below E_{fa}, which are attributed to Ce^{3+} impurities in the nominally pure compounds.

Excitation and emission spectra of K_2LaCl_5:0.1% Ce^{3+} at 10 K are shown in Fig. 7 (solid traces). The excitation spectrum of the undoped compound is reported as dotted trace for comparison. The emission spectrum shows two maxima located at 344 and 372 nm, due to transitions from the lowest energy level of the Ce^{3+} $5d$ configuration to the

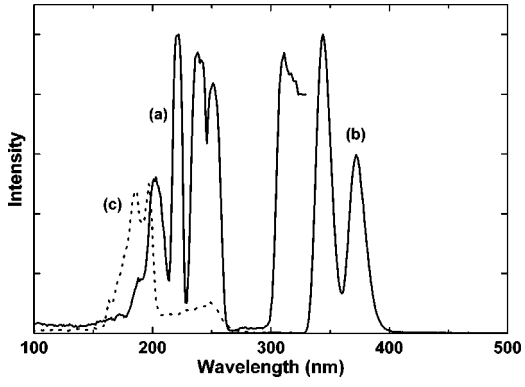

FIG. 7. (a) Excitation and (b) emission spectra of K_2LaCl_5:0.1% Ce^{3+} at 10 K. The excitation spectrum was measured at λ_{em}=372 nm, the emission spectrum was measured under λ=222 nm excitation. To compare, the excitation spectrum (c) of 415 nm emission in pure K_2LaCl_5 (dotted trace) is shown as well.

$^2F_{5/2}$ and $^2F_{7/2}$ levels, respectively. Accordingly, the ^2F spin-orbit splitting is 2190 cm^{-1}. In contrast to the x-ray excited optical luminescence spectrum shown in Fig. 3, no STE emission is excited at 222 nm.

In the excitation spectrum several bands can be distinguished. Four are located at 202, 221, 239, and 252 nm. Another band between 300 and 350 nm is actually composed of two subbands with maxima at 313 and 335 nm.[20] Based on the low symmetry of the La^{3+} site (C_s), we expect a fivefold splitting of the Ce^{3+} $5d$ levels. We assign the five lowest energy bands to the five $5d$ levels of Ce^{3+}. The data are compiled in Table II. The band at 202 nm (6.1 eV) is located just at lower energy than the exciton creation peak in the pure compound at 197 nm. It is attributed to the creation of so-called impurity-trapped excitons, i.e., an exciton created in the vicinity of a Ce^{3+} ion.

In Fig. 8 the time-integrated and time-resolved excitation and emission spectra of K_2LaBr_5:0.7% Ce^{3+} and of pure K_2LaBr_5 at 10 K are compared. The Ce^{3+} $5d\rightarrow 4f$ emission excited at 270 nm gives rise to two maxima at 357 and 388 nm [spectrum (e)]. Accordingly, the spin-orbit splitting of the ^2F ground state of Ce^{3+} is 2240 cm^{-1}. The time-integrated excitation spectrum monitoring the $5d\rightarrow 4f$ emission at 100 K is composed of two broadbands [spectrum (c)]. The band between 320 and 360 nm is composed of two subbands as in K_2LaCl_5. Spectrum (d) recorded with synchrotron radiation at 10 K shows the first band at 328 nm just before the instrumental limit was reached. The other band is assumed to be located around 345 nm, see Table II. In spectrum (d) we observe further bands between 250 and 280 nm. In the pure compound that contains trace impurities of Ce^{3+}, see spectrum (b), these bands are better resolved and clearly show two maxima at 257 and 266 nm. They are also attributed to *fd* transitions in Ce^{3+}, see Table II. The excitation peak at 294 nm in spectrum (c) may be related to an unknown impurity or to excitation of Ce^{3+} aggregates. The sharp decrease in excitation efficiency in spectrum (d) at wavelengths shorter than 255 nm (4.9 eV) is attributed to the onset of the fundamental absorption of the host crystal, see Table I. This steep drop in the 10 K spectrum is less pronounced in the 100 K spectrum (c) because the energy transfer form the host lattice to Ce^{3+} ions becomes more efficient at elevated temperatures. The fifth Ce^{3+} *fd* excitation peak remains unidentified and is probably located at shorter wavelengths than the onset of the fundamental absorption at 255 nm.

The excitation spectrum of STE emission in pure K_2LaBr_5, see Fig. 6 curve (b) and Fig. 8 curve (a), does not show clear thresholds and peaks that are required to determine E_{fa}, E_{ex}, and E_{CB}. This might be due to a poor efficiency of STE creation under across band gap excitation, but also due to the creation of impurity trapped excitons at energies below the fundamental absorption onset, since the nominally pure compounds contain impurities. In this case the sharp drop in excitation efficiency of the Ce^{3+}-doped compound at 255 nm marks E_{fa}.

The excitation and emission spectra of K_2LaI_5:0.7% Ce^{3+} at 100 K are shown in Fig. 9. The emission spectrum

TABLE II. Spectroscopic and crystallographic properties of Ce^{3+}-doped LaX_3 and K_2LaX_5, and Eu^{2+}-doped KX (X=Cl, Br, I). (N:R_{av}) represents anion coordination number and average distance to the anions (pm). Type of polyhedron (poly) and point symmetry (sym) at the Ce or Eu site are given. Values between brackets are estimated values.

Compound	(N:R_{av})	(poly:sym)	5d-excitation bands (nm)	ϵ_c (cm^{-1})	ϵ_{cfs} (cm^{-1})	Ref.
$LaCl_3$	(9:295)	(3ctp:C_{3h})	243, 250, 263, 274, 281	13000	5565	22,9
$LaBr_3$	(9:312)	(3ctp:C_{3h})	260, 270, 284, 299, 308	15906	5994	this work
LaI_3	(8:334)	(2ctp:C_{2v})	420			this work
$KCl:Eu^{2+}$	(6:315)	(octa:O_h)	2×(250), 3×(357)		12000	32
$KBr:Eu^{2+}$	(6:329)	(octa:O_h)	2×(257), 3×(357)		10900	32,33
$KI:Eu^{2+}$	(6:353)	(octa:O_h)	2×(266), 3×(357)		9500	32
K_2LaCl_5	(7:284)	(1ctp:C_s)	221, 239, 252, 313, 335	13500	15400	this work
K_2LaBr_5	(7:299)	(1ctp:C_s)	(235), 257, 266, 328, 345	(15500)	(13600)	this work
K_2LaI_5	(7:323)	(1ctp:C_s)	(263), (280), (300), 365, 380	(19100)	(11700)	this work

(b) is dominated by the characteristic doublet of Ce^{3+} 5d $\rightarrow$4f emission with peak positions at 399 and 437 nm. Accordingly, the ^2F spin-orbit splitting of the ground state of Ce^{3+} is 2180 cm^{-1}. The excitation spectrum (a) shows a broadband between 350 and 400 nm, which resembles similar bands observed for K_2LaCl_5 and K_2LaBr_5. Following the results for K_2LaCl_5 the broadband is attributed to an unresolved doublet located at approximately 365 and 380 nm, see Table II. The increasing excitation efficiency at wavelengths shorter than 320 nm (3.9 eV) is attributed to host lattice excitation.

The optical properties of $LaCl_3:Ce^{3+}$ have already been published[9,22] and data are included to Tables I and II. Figure 10 shows the optical excitation, curve (a), and emission, curve (b), spectrum of $LaBr_3$:0.5% Ce^{3+}. The Ce^{3+}5d $\rightarrow$4f emissions are located at 355 and 390 nm. Very similar to $K_2LaBr_5:Ce^{3+}$. But in contrast to the ternary halides, the five Ce^{3+}5d levels at 260, 270, 284, 299, and 308 nm in the excitation spectrum of $LaBr_3:Ce^{3+}$ are nicely resolved, see Table II. Alike $K_2LaCl_5:Ce^{3+}$, just below the onset of the fundamental absorption E_{fa} at 238 nm (5.2 eV) a clear peak is observed at 244 nm, which is attributed to impurity-trapped excitons. In the undoped $LaBr_3$ excitation spectrum, curve (c), both the Ce^{3+} *fd* bands and the impurity-trapped excitons are absent. $LaI_3:Ce^{3+}$ was studied too, but its spectroscopy is still incomplete. The two Ce^{3+} *df* emission bands are located at 450 and 500 nm. The first *fd* excitation band of Ce^{3+} was detected at 420 nm, but the four higher-lying ones are above the fundamental absorption edge of LaI_3 at 3.2 eV, and thus not accesssible.

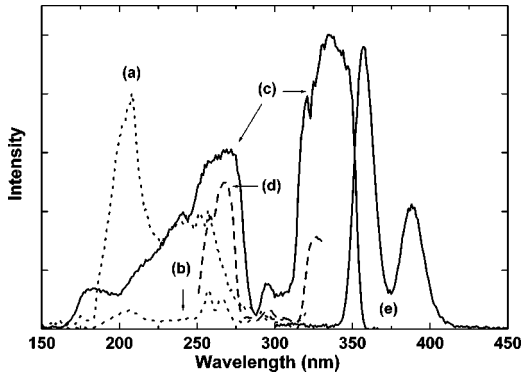

FIG. 8. (a) Slow (106 ns time gate) excitation spectrum of 400 nm emission in undoped K_2LaBr_5. (b) Fast (27 ns time gate) excitation spectrum of 355 nm emission in undoped K_2LaBr_5. (c) Time-integrated excitation spectrum of Ce^{3+} *df* emission in K_2LaBr_5:0.7% Ce^{3+} at 100 K. (d) Fast (27 ns time gate) excitation spectrum of Ce^{3+} *df* emission in K_2LaBr_5:0.7% Ce^{3+} at 10 K. (e) Time-integrated emission spectrum in K_2LaBr_5:0.7% Ce^{3+} at 270 nm excitation at 100 K.

C. Scintillation decay

Scintillation decay spectra of pure K_2LaX_5 (X=Cl, Br, I) at room temperature, excited with 662 keV γ rays from a ^{137}Cs source are shown in Fig. 11. The rising slope before $t=0$ is due to an experimental artifact and has no physical meaning. The spectra represent the luminescence intensity of the STE that decays exponentially as a function of time. The lifetime of the STE decreases along the series Cl$\rightarrow$Br$\rightarrow$I, in accordance with former observations on the alkali halides.[23] It is about 3.7 μs in the chloride, 2.2 μs in the bromide, and 350 ns in the iodide. These lifetimes do not necessarily represent the intrinsic lifetime of the STE, but can also be the

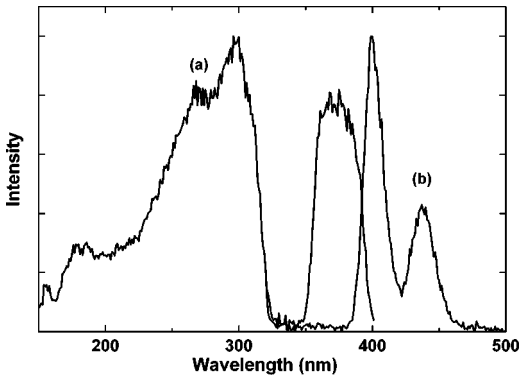

FIG. 9. (a) Excitation spectrum monitoring Ce^{3+} emission at λ_{em}=440 nm and (b) emission spectrum excited at λ_{ex}=310 nm of K_2LaI_5:0.7% Ce^{3+} at 100 K.

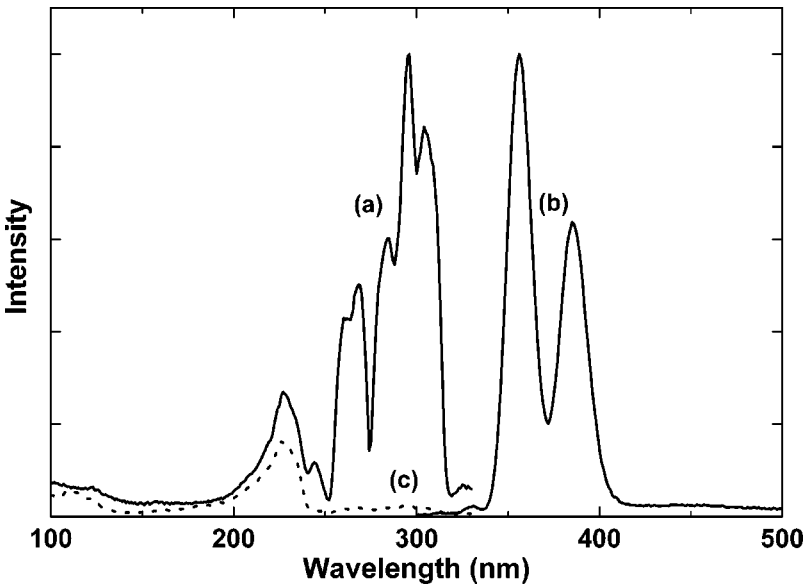

FIG. 10. (a) Excitation spectrum monitoring Ce^{3+} emission at $\lambda_{em}=360$ nm and (b) emission spectrum excited at $\lambda_{ex}=295$ nm of $LaBr_3:0.5\%$ Ce^{3+} at 10 K. To compare, the excitation spectrum (c) of the STE emission in pure $LaBr_3$ (dotted trace) is shown as well.

result of the quenching of STE luminescence at room temperature by energy migration to traps.

Figure 12 shows the scintillation decay spectra of (a) $K_2LaCl_5:0.1\%$ Ce^{3+}, (b) $K_2LaBr_5:0.7\%$ Ce^{3+}, and (c) $K_2LaI_5:0.7\%$ Ce^{3+} at room temperature. In each case, the scintillation emission is a combination of much Ce^{3+} and few STE emission, see, e.g., Fig. 3. For $K_2LaCl_5:0.1\%$ Ce^{3+} the scintillation decay profile closely resembles the spectrum of the pure compound. Despite the fact that most part of the emission originates from Ce^{3+},[20] the luminescence intensity decays exponentially with a slow decay time of about 3 μs. We assume that this represents the lifetime of the STE involved in the energy transfer from the host lattice to Ce^{3+}. In the first 100 ns after the excitation pulse $K_2LaCl_5:0.1\%$ Ce^{3+} shows an additional decay component. Its contribution to the total luminescence intensity is rather small but it increases for higher Ce concentrations.[20]

The scintillation decay of $K_2LaBr_5:0.7\%$ Ce^{3+} also consists of two components. The faster one dominates the first 0.5 μs and the slower one has a lifetime of 1.4 μs. Again the latter represents the lifetime of the STE. Finally, $K_2LaI_5:0.7\%$ Ce^{3+} shows a single fast exponential decay with a lifetime of 24 ± 1 ns. It is characteristic for the parity allowed $Ce^{3+}5d\rightarrow 4f$ transition. This fast decay component contains more than 90% of the total luminescence intensity. Apparently, the scintillation decay rates of $K_2LaX_5:Ce^{3+}$ drastically increase along the halide series from Cl to I.

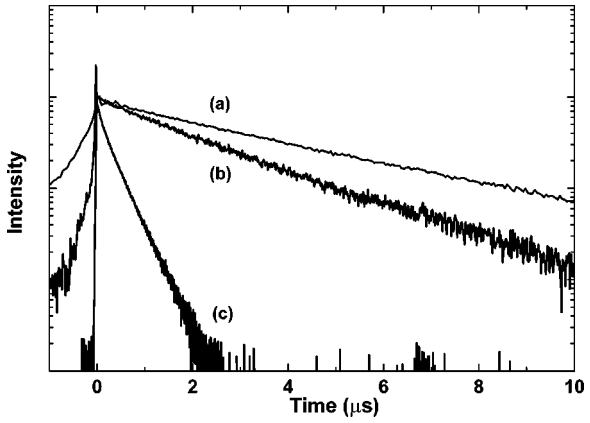

FIG. 11. Scintillation decay time spectra of (a) K_2LaCl_5, (b) K_2LaBr_5, and (c) K_2LaI_5 at room temperature.

IV. DISCUSSION

We first discuss the spectroscopic properties of the pure and Ce^{3+}-doped compounds with emphasis on the effects of anion variation. Next the scintillation mechanism of $K_2LaX_5:Ce^{3+}$ ($X=$Cl, Br, I) are discussed and compared with those of $LaX_3:Ce^{3+}$.

A. Spectroscopic properties

1. Pure compounds

Table I compiles E_{fa}, E_{ex}, and E_{CB} of the undoped crystals of LaX_3, KX, and K_2LaX_5. In addition, the emission wavelength of the self-trapped exciton is given. One may notice the following trends.

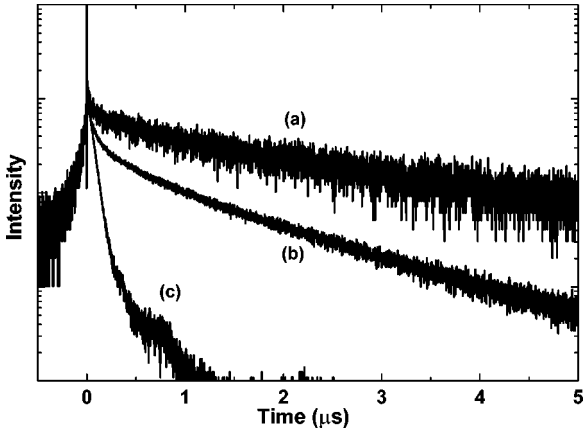

FIG. 12. Scintillation decay time spectra of (a) $K_2LaCl_5:0.1\%$ Ce^{3+}, (b) $K_2LaBr_5:0.7\%$ Ce^{3+}, and (c) $K_2LaI_5:0.7\%$ Ce^{3+} at room temperature.

(1) All three energies decrease in the sequence Cl→Br →I. This is obviously related to the decreasing electron-binding energy of the anion, which is also expressed by the Pauling electronegativity χ, i.e., 3.16, 2.96, and 2.66 for Cl, Br, and I, respectively.

(2) The tabulated energies of the alkali halides are larger than for the lanthanide halides. This must be attributed to the different Madelung potential at the trivalent La^{3+} site as compared to that at the monovalent K^+ site.

(3) The energies of the K_2LaX_5 materials resemble those of LaX_3. This illustrates that the bottom of the conduction band in both type of materials is formed by La^{3+} orbitals.

(4) For the potassium halides, the exciton-binding energy $E_{CB}-E_{ex}$ decreases in the sequence Cl→Br→I. This also holds for the alkali halides involving Li, Na, Rb, and Cs.[24] It is caused by the increasingly larger polarizability of the anion leading to a screening of the hole component of the exciton and larger effective mass m^* of the hole. Although it cannot be verified from the results in Table I, we expect for LaX_3 and K_2LaX_5 a similar behavior.

Despite that the exciton peak E_{ex} shifts 2–3 eV with type of anion in each class of compound, the position of the STE emission band does not change more than 0.4 eV in K_2LaX_5 (see Fig. 2) and LaX_3. Also in the alkali halides the anion does not have a large influence on the STE emission. Change of alkali cation from Na^+ to K^+ or Rb^+ has a much larger influence on the position of the STE emission band.[23] In these systems the energy of the STE emission band tends to decrease in the series Na^+ to K^+ to Rb^+.

2. Ce^{3+} spectroscopy

For the free Ce^{3+} ion, the $5d$ configuration is located at an average energy of 51 230 cm^{-1}.[8] Due to the spin-orbit interaction two energy levels, i.e., $^2D_{3/2}$ and $^2D_{5/2}$, are observed. Note, in this section we will use, as is commonly done so in spectroscopy, the inverse wavelength in cm^{-1} as the unit of energy (1 eV=8065 cm^{-1}).

In a crystalline environment, the average energy of the $5d$ configuration is reduced by the centroid shift, ϵ_c. Depending on the site symmetry the degeneracy might be lifted and up to five distinct $5d$ energy levels are obtained. The energy difference between the lowest and highest $5d$ level is defined as the total crystal field splitting ϵ_{cfs}. Table II compiles the wavelengths λ_i of the five $4f\rightarrow5d$ excitation bands of Ce^{3+} in the LaX_3 and K_2LaX_5 compounds.

Figure 13 illustrates how the $5d$ crystal field splitting in Ce^{3+} varies with the shape and size of the anion coordination polyhedron around Ce^{3+}. The size of the polyhedron is modeled by the average distance R_{av} of the cation to the N coordinating anions, see column 2 in Table II. A correction of $0.6\Delta R$ was applied to account for the lattice relaxation. ΔR is defined as the difference in ionic radius between Ce^{3+} and the cation it substitutes for. It amounts to 2, 3, and 37 pm for LaX_3, K_2LaX_5, and KX, respectively. Empirically, ϵ_{cfs} can be modeled by Eq. (1):

$$\epsilon_{cfs}=\beta_{poly}R_{av}^{-2}, \qquad (1)$$

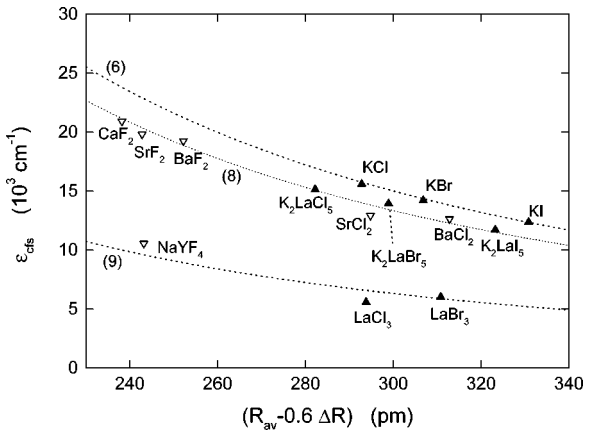

FIG. 13. The crystal field splitting ϵ_{cfs} of the Ce^{3+} $5d$ configuration in compounds as a function of the average distance to neighboring anions in the relaxed lattice. Dashed curves marked (6), (8), and (9) pertain to sixfold octahedral, eightfold cubic, and ninefold tricapped trigonal prism coordination. Values for KCl, KBr, and KI are anticipated from Eu^{2+} data.

where β_{poly} is a constant depending on the shape of the coordination polyhedron.[10] The validity of Eq. (1) for CaF_2, SrF_2, BaF_2, $SrCl_2$, and $BaCl_2$ with eightfold cubic coordination, and $NaYF_4$, $LaCl_3$, and $LaBr_3$ with ninefold tricapped trigonal prismatic (3ctp) coordination is demonstrated by the dashed lines in Fig. 13.

The total crystal field splitting in K_2LaCl_5 is about the same as the value typical for cubic coordination, see Fig. 13. Information on K_2LaBr_5 and K_2LaI_5 is still incomplete, but reasonable estimates for the missing $5d$ level energies can be given. The type of coordination polyhedron in the K_2LaX_5 compounds are the same, and then an R^{-2} dependence with polyhedral size is expected. Employing Eq. (1) the total crystal field splitting and from that the wavelengths of the missing $5d$ bands were estimated. They are given together with the values for the centroid shift ϵ_c within brackets in columns 4–6 of Table II.

Information is not available on the energy of Ce^{3+} $5d$ levels in the KX type of compounds. However, it can be estimated from the results available on the energies of the $4f^6 5d$ levels of Eu^{2+} in these compounds. The $5d$ levels of Eu^{2+} at sites with octahedral (octa) coordination are split into a low-energy triplet and a high-energy doublet state separated by an energy known as the $10Dq$ value, which can be set equal to ϵ_{cfs}. From previous studies it is known that the crystal field splitting in Eu^{2+} is about 0.77 times that in Ce^{3+}.[10] Using this ratio, the data anticipated for Ce^{3+}-doped KX compounds is drawn in Fig. 13.

We now observe that the (anticipated) crystal field splitting in the K_2LaX_5 compounds falls between that of octahedral and cubic coordination. This agrees with the general trend of decreasing crystal field splitting with larger coordination number N around Ce^{3+}. It is largest for octahedral coordination with $N=6$. Provided that the so-called prismatic angle remains the same, the crystal field splitting for a trigonal prism coordination is the same as for octahedral coordination.[10,25] Adding one capping anion on one of the

three side faces of a trigonal prism, as in K_2LaX_5, leads to a smaller crystal field splitting, but apparently still somewhat larger than that of cubic coordination. When all three side faces of the trigonal prism are capped with an anion, one obtains the situation in $NaYF_4$, $LaCl_3$, and $LaBr_3$ with much reduced crystal field splitting. Note that the changing chemical properties of the anions in the sequence Cl to Br to I are not important for the crystal field splitting. Only the change in ionic radius appears via R_{av} in Eq. (1).

On the other hand, for fluorides, chlorides, bromides, and iodides, ϵ_c is typically 6000 cm^{-1}, 14 000 cm^{-1}, 16 000 cm^{-1}, and 19 000 cm^{-1}, respectively. This is also revealed in Table II

B. STE and scintillation properties

When the electron and hole components of a STE recombine, STE luminescence is observed. This luminescence usually arises from a spin-forbidden transitions made partly allowed by the halogen spin-orbit interaction of the V_K core of the STE, but still the decay time is relatively large.

On the other hand, the $Ce^{3+}5d \rightarrow 4f$ emission is spin and dipole allowed and has a short decay time of $(2-6) \times 10^{-8}$ s. After absorbing a γ-ray quantum in the host crystal, free electrons and holes are created in the conduction band and valence band, respectively. If these free electrons and holes are trapped promptly by a Ce^{3+} ion before STE formation, the scintillation decay time will be the same as the characteristic lifetime of the $5d$ excited state of Ce^{3+}. This is the situation at room temperature in $LaBr_3$:0.5% Ce^{3+} and in K_2LaI_5:0.7% Ce^{3+}, e.g., Fig. 12(c). Otherwise, slow scintillation is observed due to STE luminescence and energy transfer from the (migrating) STE towards Ce^{3+}.

As can be seen from Fig. 11, the lifetime of the STE tends to become shorter in the series Cl→Br→I. This can be satisfactorly accounted for in terms of the larger spin-orbit interaction in the heavier halides,[26] leading to a more allowed transition. However, the smaller values for the lifetime of the STE can also be explained by the increasing thermally activated hopping rate of the STE in the series Cl→Br→I.[27,28] It leads to quenching of STE emission and decreasing lifetime due to the energy transfer to defects or Ce^{3+}.

In principle, there are several energy transfer mechanisms possible that may account for the observed correlation between the decay time of the scintillation pulse and the type of anion. In the case of *STE diffusion*, the luminescence of K_2LaX_5:Ce^{3+} (X=Cl, Br, I) at low temperatures is largely due to the radiative recombination of the STE, see Fig. 3. However, as the temperature rises the mobility of the STE increases as well, and the energy is transferred to a Ce^{3+} center when the STE encounters a Ce^{3+} ion. Such an energy transfer can explain the observed anticorrelation of Ce^{3+} and STE luminescence intensity in Figs. 4 and 5 between 100 and 400 K. If we consider the migration of a V_K center through the lattice, the activation energy for V_K diffusion decreases from Cl to I.[29–31] In the same order the mobility of the STE increases. Indeed, the scintillation decay time decreases from K_2LaCl_5:0.1% Ce^{3+} (Ref. 20) to K_2LaBr_5:0.7% Ce^{3+} to K_2LaI_5:0.7% Ce^{3+} (see Fig. 12).

V. SUMMARY AND CONCLUSIONS

In this work the spectroscopic properties and scintillation mechanism of undoped and Ce^{3+}-doped K_2LaX_5, LaX_3, and KX (X=Cl, Br, I) have been determined and compared with each other. The band gap E_{CB}, the energy of the exciton peak E_{ex}, and the wavelength of STE emission λ_{STE} are very similar for K_2LaX_5 and LaX_3, but much different from KX. The conduction band levels of La^{3+} are at 1–2 eV lower energy than those of K^+. The decreasing binding strength for electrons along the halide series results in a band gap reduction of about 2 eV from Cl to I in each series of compounds.

The energy of the five *fd* transitions of Ce^{3+} in LaX_3 and K_2LaX_5 compounds was determined by excitation and emission spectroscopy. The highest energy transitions of K_2LaBr_5 and K_2LaI_5 are located beyond the fundamental absorption of the host crystals. For those cases the energies were estimated based on empirical data from other Ce^{3+}-doped compounds. Since Ce^{3+}-doped KX has not been studied, the Ce^{3+} $5d$ crystal field splitting was derived from data on Eu^{2+}-doped KX. For a given Ce^{3+} coordination, the increasing ionic radius of the anions from Cl to I causes a 20% decrease of the crystal field splitting. On the other hand, the centroid shift of the $5d$ configuration increases in the sequence Cl, Br, I, due to larger covalency between anion and Ce^{3+} and due to larger polarizability of the anion.

Across the bandgap excitations either by x rays, γ rays, or synchrotron radiation result in a combination of $Ce^{3+}5d \rightarrow 4f$ and STE emission. The ratio of Ce^{3+} to STE emission intensity depends on temperature and Ce^{3+} concentration. Clear trends are observed. For low concentrations of 0.2–0.5 % and increasing temperature from 100 to 400 K, the Ce^{3+} emission gains intensity at the expense of the STE emission. This is very clear for $LaCl_3$ and K_2LaCl_5 where the STE emission dominates at 100 K, and it is fully transferred to the Ce^{3+} emission at 400 K.[20,18] At room temperature both emissions are still present. Along the series Cl, Br, I the intensity of the Ce^{3+} emission increases at the expense of STE emission. In $LaBr_3$ and K_2LaI_5 with 0.2–0.5% Ce^{3+}, the STE emission is very weak at room temperature and only fast Ce^{3+} *df* emission is observed. These two compounds provide efficient and fast scintillators already at small Ce^{3+} concentrations. $LaCl_3$ and K_2LaCl_5 are fast and efficient scintillators only when the Ce^{3+} concentration is increased above 10%. The increase of Ce^{3+} scintillation efficiency and scintillation speed along the series from Cl to I is attributed to (1) an increasing hopping mobility of STEs and (2) the higher trapping rate of free electrons and holes by Ce^{3+} relative to the STE creation rate.

ACKNOWLEDGMENTS

This work was supported by the Netherlands Technology Foundation (STW), the Swiss National Science Foundation, IHP Contract No. HPRI-CT-1990-00040 of the European Commission, and Saint-Gobain Cristeaux et Détecteurs.

[1] A.J. Wojtowicz, M. Balcerzyk, E. Berman, and A. Lempicki, Phys. Rev. B **49**, 14 880 (1994).
[2] A.J. Wojtowicz, P. Szupryczynski, J. Glodo, W. Drozdowski, and D. Wisniewski, J. Phys.: Condens. Matter **12**, 4097 (2000).
[3] A. Lempicki and J. Glodo, Nucl. Instrum. Methods Phys. Res. A **416**, 333 (1998).
[4] C. Pedrini, C. Dujardin, J.C. Gacon, A.N. Belsky, A.N. Vasilev, and A.G. Petrosyan, Radiat. Eff. Defects Solids **154**, 277 (2001).
[5] E.V.D. van Loef, P. Dorenbos, C.W.E. van Eijk, K. Krämer, and H.U. Güdel, Appl. Phys. Lett. **77**, 1467 (2000).
[6] E.V.D. van Loef, P. Dorenbos, C.W.E. van Eijk, K. Krämer, and H.U. Güdel, Appl. Phys. Lett. **79**, 1573 (2001).
[7] E.V.D. van Loef, P. Dorenbos, and C.W.E. van Eijk, J. Phys.: Condens. Matter **15**, 1367 (2003).
[8] P. Dorenbos, Phys. Rev. B **62**, 15 640 (2000).
[9] P. Dorenbos, Phys. Rev. B **62**, 15 650 (2000).
[10] P. Dorenbos, J. Alloys Compd. **341**, 156 (2002).
[11] R.T. Williams and K.S. Song, J. Phys. Chem. Solids **51**, 679 (1990).
[12] G. Meyer, Inorg. Synth. **25**, 146 (1989).
[13] J.B. Reed, B.S. Hopkins, and L.F. Audrieth, Inorg. Synth. **1**, 28 (1936).
[14] G. Meyer, *Synthesis of Lanthanide and Actinide Compounds*, edited by G. Meyer and L. Morss (Kluwer, Dordrecht, 1991), p. 145.
[15] G. Meyer, J. Soose, A. Moritz, V. Vitt, and Th. Holljes, Z. Anorg. Allg. Chem. **521**, 161 (1985).
[16] G. Zimmerer, Nucl. Instrum. Methods Phys. Res. A **308**, 178 (1991).
[17] W.W. Moses, Nucl. Instr. Meth. A **336**, 253 (1993).
[18] O. Guillot-Noël, J.T.M. de Haas, P. Dorenbos, C.W.E. van Eijk, K. Krämer, and H.U. Güdel, J. Lumin. **85**, 21 (1999).
[19] E.V.D. van Loef, P. Dorenbos, C.W.E. van Eijk, K. Krämer, and H.U. Güdel, IEEE Trans. Nucl. Sci. **48**, 341 (2001).
[20] J.C. van't Spijker, P. Dorenbos, C.W.E. van Eijk, K. Krämer, and H.U. Güdel, J. Lumin. **85**, 1 (1999).
[21] E.V.D. van Loef, P. Dorenbos, C.W.E. van Eijk, K.W. Krämer, and H.U. Güdel, Nucl. Instrum. Methods Phys. Res. A **486**, 254 (2002).
[22] J. Andriessen, O.T. Antonyak, P. Dorenbos, P.A. Rodnyi, G.B. Stryganyuk, C.W.E. van Eijk, and A.S. Voloshinovskii, Opt. Commun. **178**, 355 (2000).
[23] K. Kan'no, K. Tanaka, and T. Hayashi, Rev. Solid State Sci. **4**, 383 (1990).
[24] K.S. Song and R.T. Williams, in *Self-Trapped Excitons*, edited by M. Cardona, Springer Series on Solid-State Sciences Vol. 105 (Springer-Verlag, New York, 1993).
[25] C. Görller-Walrand and K. Binnemans, in *Handbook on the Physics and Chemistry of Rare Earths*, edited by K. A. Gschneidner, Jr. and L. Eyring (Elsevier Science B.V., Amsterdam, 1996), Vol. 23, Chap. 155.
[26] M.N. Kabler and D.A. Patterson, Phys. Rev. Lett. **19**, 652 (1967).
[27] L.F. Chen, K.S. Song, and C.H. Leung, Nucl. Instrum. Methods Phys. Res. B **46**, 216 (1990).
[28] K. Tanimura and N. Itoh, J. Phys. Chem. **42**, 901 (1981).
[29] G. Ascarelli and R.H. Sturen, Phys. Rev. B **11**, 4045 (1975).
[30] T. Lida and R. Monnier, Phys. Status Solidi B **74**, 91 (1976).
[31] R. Monnier, K.S. Song, and A.M. Stoneham, J. Phys. C **10**, 4441 (1979).
[32] J.A. Hernandez, F.J. Lopez, H.S. Murrieta, and J.O. Rubio, J. Phys. Soc. Jpn. **50**, 225 (1981).
[33] M.G. Aguilar, J.O. Rubio, F.J. Lopez, J. Garcia-Sole, and H. Murrieta, Solid State Commun. **44**, 141 (1982).